

# **SANDIA REPORT**

SAND2002-2949

Unlimited Release

Printed September 2002

## **SAR Window Functions: A Review and Analysis of the Notched Spectrum Problem**

Fred M. Dickey, Louis A. Romero, and Armin W. Doerry

Prepared by

Sandia National Laboratories

Albuquerque, New Mexico 87185 and Livermore, California 94550

Sandia is a multiprogram laboratory operated by Sandia Corporation, a Lockheed Martin Company, for the United States Department of Energy under Contract DE-AC04-94AL85000.

Approved for public release; further dissemination unlimited.



**Sandia National Laboratories**

Issued by Sandia National Laboratories, operated for the United States Department of Energy by Sandia Corporation.

**NOTICE:** This report was prepared as an account of work sponsored by an agency of the United States Government. Neither the United States Government, nor any agency thereof, nor any of their employees, nor any of their contractors, subcontractors, or their employees, make any warranty, express or implied, or assume any legal liability or responsibility for the accuracy, completeness, or usefulness of any information, apparatus, product, or process disclosed, or represent that its use would not infringe privately owned rights. Reference herein to any specific commercial product, process, or service by trade name, trademark, manufacturer, or otherwise, does not necessarily constitute or imply its endorsement, recommendation, or favoring by the United States Government, any agency thereof, or any of their contractors or subcontractors. The views and opinions expressed herein do not necessarily state or reflect those of the United States Government, any agency thereof, or any of their contractors.

Printed in the United States of America. This report has been reproduced directly from the best available copy.

Available to DOE and DOE contractors from  
U.S. Department of Energy  
Office of Scientific and Technical Information  
P.O. Box 62  
Oak Ridge, TN 37831

Telephone: (865)576-8401  
Facsimile: (865)576-5728  
E-Mail: [reports@adonis.osti.gov](mailto:reports@adonis.osti.gov)  
Online ordering: <http://www.doe.gov/bridge>

Available to the public from  
U.S. Department of Commerce  
National Technical Information Service  
5285 Port Royal Rd  
Springfield, VA 22161

Telephone: (800)553-6847  
Facsimile: (703)605-6900  
E-Mail: [orders@ntis.fedworld.gov](mailto:orders@ntis.fedworld.gov)  
Online order: <http://www.ntis.gov/ordering.htm>



SAND2002-2949  
Unlimited Release  
Printed September 2002

# **SAR Window Functions: A Review and Analysis of the Notched Spectrum Problem**

Fred M. Dickey  
Firing Set & Optical Engineering Department

Louis A. Romero  
Computational Math/Algorithms Department

Armin W. Doerry  
Radar and Signals Analysis Department

Sandia National Laboratories  
PO Box 5800  
Albuquerque, NM 87185

## **ABSTRACT**

Imaging systems such as Synthetic Aperture Radar collect band-limited data from which an image of a target scene is rendered. The band-limited nature of the data generates sidelobes, or 'spilled energy' most evident in the neighborhood of bright point-like objects. It is generally considered desirable to minimize these sidelobes, even at the expense of some generally small increase in system bandwidth. This is accomplished by shaping the spectrum with window functions prior to inversion or transformation into an image. A window function that minimizes sidelobe energy can be constructed based on prolate spheroidal wave functions. A parametric design procedure allows doing so even with constraints on allowable increases in system bandwidth. This approach is extended to accommodate spectral notches or holes, although the guaranteed minimum sidelobe energy can be quite high in this case. Interestingly, for a fixed bandwidth, the minimum-mean-squared-error image rendering of a target scene is achieved with no windowing at all (rectangular or boxcar window).

## **ACKNOWLEDGEMENTS**

We would like to thank Stephen E. Yao for help with the figures for this report.

This work was performed as part of the Advanced Radar Systems (ARS) and Concealed Target Synthetic Aperture Radar (CTSAR) projects, sponsored by the US Department of Energy, NNSA/NA-22 Proliferation Detection program office, under supervision of Randy Bell.

# FOREWORD

Synthetic Aperture Radar systems are being driven to provide images with ever finer resolutions. The General Atomics Ku-band Lynx SAR currently provides 4-inch resolution images, and systems on the drawing board are being asked to provide at least this and often even finer resolutions. This, of course, requires ever wider bandwidths to support these resolutions and often in other frequency bands across the microwave (and lower) spectrum.

The problem is that the spectrum is already quite crowded with a multitude of users, and a multitude of uses. The FCC undoubtedly faces enormous pressures to minimize interference between the various spectral users. For a radar system, this manifests itself as a number of ‘stay-out’ zones in the spectrum; frequencies where the radar is not allowed to transmit. Even frequencies where the radar is allowed to transmit might be corrupted by interference from other legitimate (and/or illegitimate) users, rendering these frequencies useless to the radar system. In a SAR image, these spectral holes (by whatever source) degrade images, most notably by increasing objectionable sidelobe levels.

For contiguous spectrums, sidelobes in SAR images are controlled by employing window functions. However, those windows that work well for contiguous spectrums don’t seem to work well for spectrums with significant gaps or holes. The investigation reported herein was commissioned with the question “Can some sorts of window functions be developed and employed to advantage when the spectrum is not contiguous, but contains significant holes or gaps?”

This page left intentionally blank.

# CONTENTS

1 Introduction.....	9
2 Maximum Energy Windowing .....	11
2.1 The solution for a Contiguous Passband.....	11
2.2 Comparison to the Taylor Window.....	18
3 Maximum Energy Windowing With Stop-Bands.....	22
3.1 Solution for the Centered Stop-Bands .....	24
3.2 Perturbation Theory .....	34
3.3 The Iteration.....	38
3.4 Alternatives to Windowing for Sidelobe Control .....	43
4 Least squares Reconstruction.....	44
5 Summary .....	46
Appendix A.....	47
Appendix B .....	49
References.....	51

This page left intentionally blank.

# 1 Introduction

Imaging systems such as Synthetic Aperture Radar collect band-limited data from which an image of a target scene is rendered. The band-limited nature of the data generates sidelobes, or ‘spilled energy’ most evident in the neighborhood of bright point-like objects. It is generally considered desirable to minimize these sidelobes, or at least reduce them to some more tolerable level. An image quality specification might limit the peak sidelobe level in comparison to the mainlobe response, and further limit the relative energy outside of the mainlobe. This is often desirable even at the expense of requiring some generally small increase in system bandwidth, or alternately suffering some degradation in image resolution. This is accomplished by shaping the spectrum with window functions prior to inversion or transformation into an image. A myriad of window functions exist in the literature, all with different attributes, and each with its proponents.<sup>1</sup>

Wideband imaging systems are often prohibited from using a contiguous spectrum, thereby forced to deal with perhaps one or more spectral notches or regions of missing data. Even relatively small notches of perhaps ten percent of the overall bandwidth can degrade the image with substantially enhanced objectionable sidelobes. A fundamental question arises that “Can window functions be developed to minimize sidelobe levels for data containing spectral notches?”

The purpose of this study is to investigate the merits of using a maximum energy constraint as a basis for the development of windows for a spectrum that contains one or more notches (stop-bands). The maximum energy constraint consists of seeking a solution for a window that maximizes the energy in an interval equal to or greater than

the resolution (in some cases the interval could be less than the resolution). This approach is based on the idea that maximizing the energy in an interval, or equivalently minimizing the energy outside the interval, tends to strongly minimize the peak-to-sidelobe ratio. Clearly as the energy outside the interval approaches zero, the peak-to-sidelobe ratio would approach infinity. This approach has had some success in edge enhancement filter design.<sup>2,3</sup> The maximum energy criterion is basic, straightforward, and offers an intuitive appeal. Nevertheless we do not know of its prior application to the windowing problem. In the next section we investigate the potential of the maximum energy criterion by applying it to the standard windowing problem. The maximum energy solution is compared to the standard Taylor window, and it is shown that the Taylor window compares favorably with the rigorously derived Maximum Energy window. In Section 3 we apply the maximum energy criterion to the problem of SAR data with stop-bands. Numerical solutions to the resulting integral equation are presented. Section 4 briefly addresses the interesting, but not commonly recognized, fact that the minimum-mean-squared-error imaging of the target scene precludes windowing of the data. Finally, a brief summary of the paper is given in Section 5. Although the analysis in this report was developed specifically for the SAR problem, it is generally applicable to multiple aperture optical telescopes and antenna arrays for radio astronomy.

## 2 Maximum Energy Windowing

While the intent of this paper is to deal with data containing spectral notches, it is reasonable (and instructive) to ask “What about the case of no notches at all, that is, a contiguous passband?” This is the traditional windowing problem. As a precursor to dealing with spectral notches, we next develop the Maximum Energy window for the contiguous spectrum case and compare it to a more familiar Taylor window.

### 2.1 The Solution for a Contiguous Passband

The solution to the simple windowing problem is readily obtained in terms of prolate spheroidal wave functions. They are especially suited to the problems involving simultaneous constraints on the space-width and bandwidth of a function.<sup>4,5,6,7,8</sup> For convenience we give the main properties of the prolate spheroidal wave functions,  $\mathbf{y}_n(x)$ , here.

1) The  $\mathbf{y}_n(x)$  are band-limited, orthonormal on the real line and complete in the space of band-limited functions (bandwidth  $2W$ ):

$$\int_{-\infty}^{\infty} \mathbf{y}_i(x) \mathbf{y}_j(x) dx = \begin{cases} 0, & i \neq j \\ 1 & i = j \end{cases}. \quad (1)$$

2) The  $\mathbf{y}_n(x)$  are orthogonal and complete on the interval  $-X/2 \leq x \leq X/2$ :

$$\int_{-X/2}^{X/2} \mathbf{y}_i(x) \mathbf{y}_j(x) dx = \begin{cases} 0, & i \neq j \\ \mathbf{I}_i & i = j \end{cases}. \quad (2)$$

3) For all values of  $x$ , real or complex,

$$\mathbf{I}_n \mathbf{y}_n(x) = \int_{-x/2}^{x/2} \frac{\sin 2\mathbf{p}W(x-y)}{\mathbf{p}(x-y)} \mathbf{y}_n(y) dy. \quad (3)$$

4) The  $\mathbf{I}_n$  are real and positive with the property,

$$1 > \mathbf{I}_0 > \mathbf{I}_1 > \mathbf{I}_2 > \dots \quad (4)$$

This notation conceals the fact that both the  $\mathbf{y}$ 's and the  $\mathbf{I}$ 's are functions of the product  $WX$ . That is,  $\mathbf{I}_n = \mathbf{I}_n(c)$  and  $\mathbf{y}_n(x) = \mathbf{y}_n(c, x)$ , where

$$c = \mathbf{p}WX. \quad (5)$$

Equivalently, the  $\mathbf{y}_n(x)$  can be defined as

$$i\Omega \sqrt{\frac{\mathbf{I}_n(c)}{2\mathbf{p}c}} \mathbf{y}_n(c, x) = \frac{1}{2\mathbf{p}} \int_{-\Omega}^{\Omega} e^{i\mathbf{w}x} \mathbf{y}_n(c, \mathbf{w}X/2\Omega) d\mathbf{w}, \quad (6)$$

where we have used the notation of Slepian and Pollak.<sup>4</sup> In terms of the previous notation,  $\Omega = 2\mathbf{p}f$  and  $2c = \Omega X$ . Taking the Fourier transform of both sides of Eq. (6) makes explicit the band-limited nature of the prolate spheroidal wave functions. We will use this notation in what follows.

We can define the simple windowing problem as finding the band-limited function,  $f(x)$ , that maximizes the energy ratio

$$E = \frac{\int_{-x/2}^{x/2} |f(x)|^2 dx}{\int_{-\infty}^{\infty} |f(x)|^2 dx}. \quad (7)$$

Using 1) we can write the solution to the problem as

$$f(x) = \sum_n a_n \mathbf{y}_n(x). \quad (8)$$

Substituting Eq. (8) in Eq. (7) and using Eqs. (1) and (2) gives

$$E = \frac{\sum_n I_n |a_n|^2}{\sum_n |a_n|^2}. \quad (9)$$

It is easily established, using 4), that Eq. (7) is a maximum for

$$f(x) = a_0 \mathbf{y}_0(x), \quad (10)$$

where  $a_0$  is arbitrary, and the maximum fractional energy is

$$E_{\max} = I_0. \quad (11)$$

It remains to relate this solution to that for the non-windowed sinc function response. Specifically the problem is to compare bandwidths. To do this we have computed  $\mathbf{y}_0(c)$  for  $c = 0.5, 1.0, 2.0, 3.0, 4.0, 5.0, 6.0, 7.0, 8.0, 9.0,$  and  $10.0$ . Four prolate spheroidal wave functions are shown in Fig. 1 for  $c = 0.5, 1.0, 2.0,$  and  $4.0$ . The remaining functions are reproduced in Fig A-1 and Fig A-2 in Appendix A for completeness. We have written a Tchebychev collocation program to numerically obtain the eigenvalues and eigenfunctions of the integral equation defining the prolate spheroidal wave functions. We do not know of a literature source for the curves beyond those shown in Fig. 1. It can

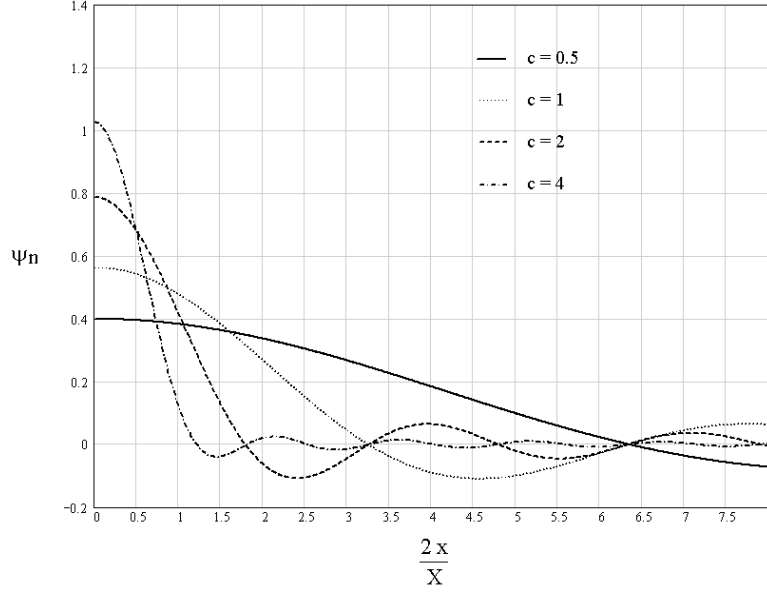


Fig. 1 Four prolate spheroidal wave functions for  $c = 0.5, 1.0, 2.0, 4.0$ .

be seen that, for the functions plotted the functions narrow and the peak-to-sidelobe ratio increases with increasing  $c$ . The space-bandwidth-product,  $c$ , is well defined for the prolate spheroidal wave functions; however, its definition is generally arbitrary. For example, if one is interested in the uncertainty principle, root-mean-square widths are appropriate. We can define  $c$  for the sinc function as  $c = x_0 \Omega = p$  where  $x_0$  is the distance to the first zero of the sinc function. In terms of the half-power width of the sinc function, we have

$$\Omega_s = \frac{.88p}{X_s}, \tag{12}$$

where  $X_s$  is the full width at the half-power points. The value of  $c$  for the solution given by Eq. (10) is arbitrary. The problem is to now relate this to the bandwidth of the prolate spheroidal wave function.

We look for a solution where the half-power points fall in the interval  $X$  and the peak-to-sidelobe ratio is acceptable. For the data in Fig. 1, the curve for  $c = 4$  is close. For this curve, the peak-to-sidelobe ratio is  $R_{ps} = 28.2$  dB. The energy ratio given by Eq. (7) can be computed from tables of eigenvalues<sup>6</sup> to be  $E = 0.99588549$ , which corresponds to a ratio of the energy in the interval to energy outside the interval to be 23.8 dB. The bandwidths of the sinc function and the prolate wave function can be related by considering solutions with the same half-power widths. It can be seen from the  $c = 4$  curve in Fig. 1 that  $c$  is given by (approximately)  $c = \Omega X' = 4$ , where  $X'$  is the full width at the half-power points for  $\mathbf{y}_0$ . This gives

$$\Omega_{ps} = \frac{4}{X'}. \quad (13)$$

The ratio of the bandwidths can be obtained by equating  $X$  and  $X'$ , giving

$$\frac{\Omega_{ps}}{\Omega_s} = \frac{4}{.88p} = 1.45. \quad (14)$$

This is the amount that the bandwidth must be increased to implement a maximum energy windowing corresponding to  $c = 4$ . Increasing  $c$  would result in a further improvement in the peak-to-sidelobe ratio and energy ratio at the expense of increased bandwidth. The relation is not linear. The peak-to-sidelobe ratio is plotted as a function of  $c$  in Fig. 2. The slope of the curve in the linear portion is approximately 7. In the next section we compare the energy ratio for this approach to that for the Taylor window.

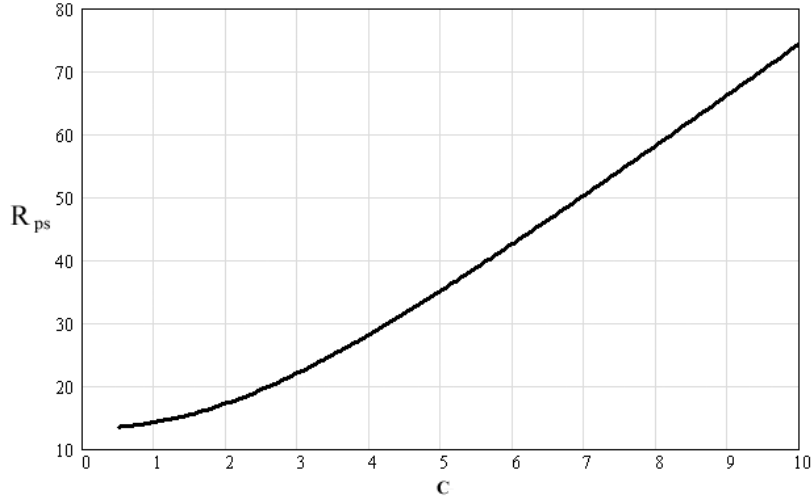


Fig. 2 Peak-to-sidelobe ratio (in dB) as a function of  $c$  for prolate spheroidal wave function windowing.

Using Eq. 7 and Eq. 11 we can write the ratio of the energy in the interval  $X$  to that outside the interval  $X$  as

$$R = \frac{I(c)}{1-I(c)}. \quad (15)$$

The energy ratio of Eq. 15 is plotted in Fig. 3. It can be seen from the figure that there is an approximate 8 dB gain in the energy ratio for each integer increase in  $c$ .

In the argument leading to Eq. 14 for the relative bandwidths of the sinc functions and the prolate spheroidal wave functions we needed to relate the half power widths for the prolate spheroidal wave functions to the to the interval  $X$ . This relation is plotted in Fig. 4 as  $c$  ranges from 0.5 to 10. In the figure  $x$  is plotted relative to the unit interval ( $X = 1$ ).

A maximum energy windowing design for specific SAR resolution/bandwidth parameters is given in Appendix B. In the appendix, an algorithm is given for

determining the value of  $c$  and a plot of the windowing function,  $y_0(c, x)$ , which is also the impulse response when appropriately scaled.

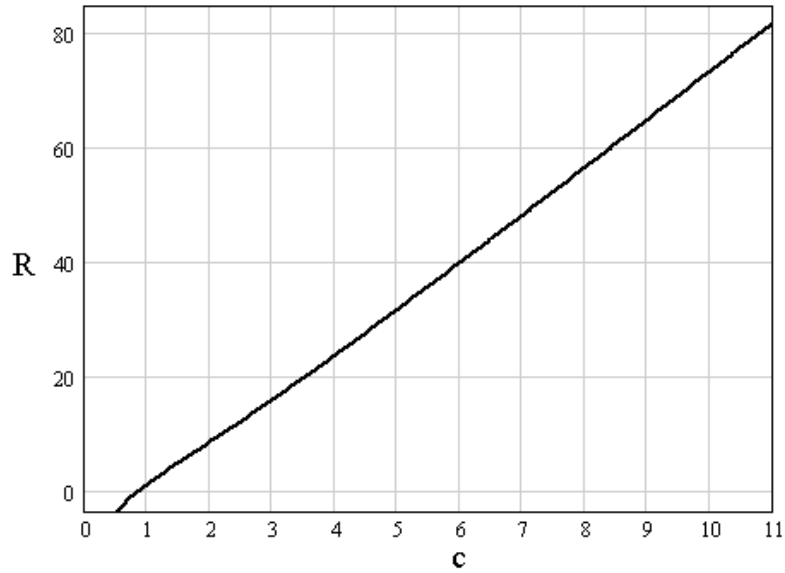


Fig. 3 The ratio of the energy in the interval X to the energy outside the interval (in dB).

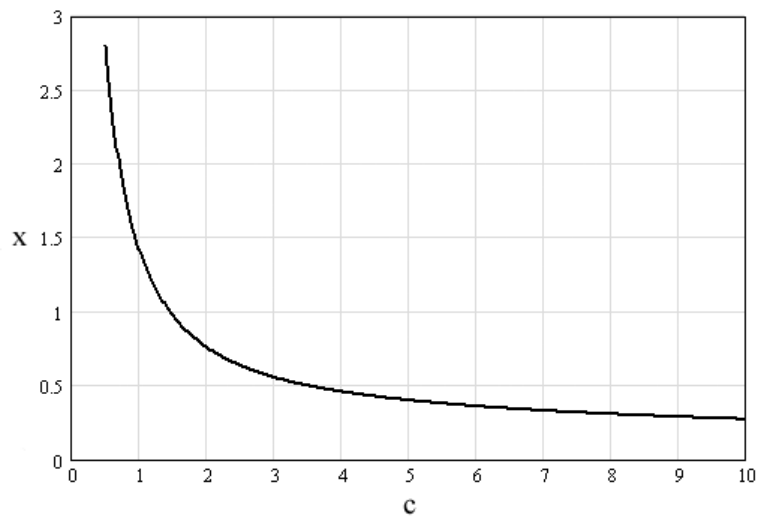


Fig. 4 Half-power point relative to the unit interval.

## 2.2 Comparison to the Taylor Window

A window function that minimizes mainlobe width while maintaining a peak sidelobe constraint is the Dolph-Tschebysheff window.<sup>9</sup> A popular window function for Synthetic Aperture Radar data processing is the Taylor window. The Taylor window approximates the Dolph-Tschebysheff window near its mainlobe, but unlike the Dolph-Tschebysheff window allows sidelobes to decay at a  $1/f$  rate beyond some distance from the mainlobe.<sup>10</sup> Sidelobe levels and the point beyond which sidelobes roll off are parameters to the Taylor window.

As a reference, we choose the Taylor window with peak sidelobe value of  $-35$  dBc (dB with respect to the center of the mainlobe), and  $nbar = 4$ . This window requires a bandwidth extension of approximately 1.18 to maintain a mainlobe half-power point equal to  $1/2$  the distance from the origin to the first zero of the corresponding sinc function (before bandwidth extension). Appendix B discusses the selection of a corresponding Maximum Energy window, and presents a solution with parameter  $c = 4.1432$ . These windows are compared in Fig. 5.

Corresponding impulse responses are shown in Fig. 6 along with a typical SAR sidelobe limit specification.

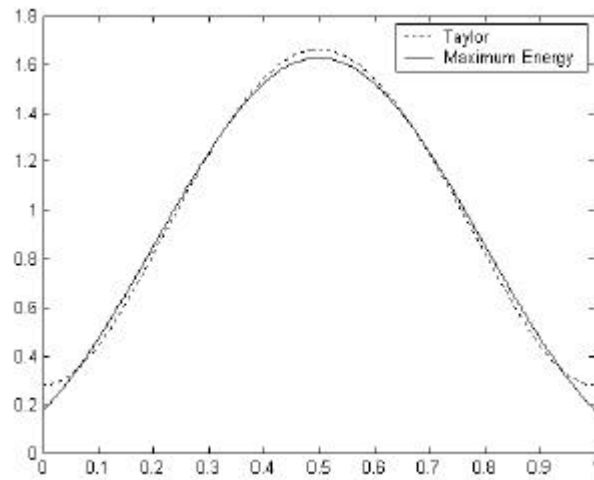


Fig. 5 Comparison of the Taylor window with the Maximum Energy window.

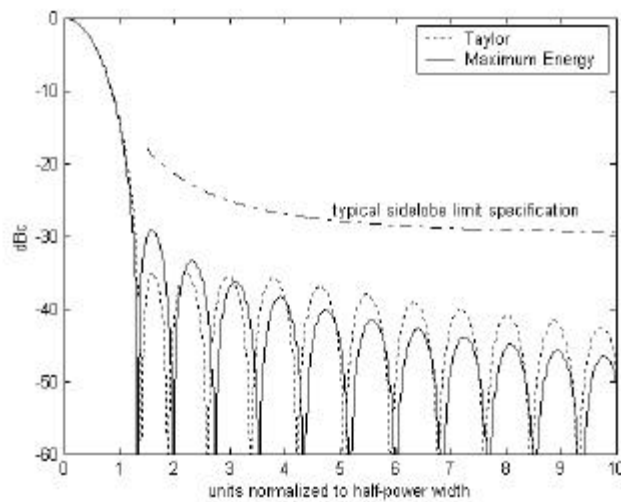


Fig. 6 Comparison of impulse responses (magnitudes) for the Taylor window and the Maximum Energy window.

A cursory comparison shows that the impulse response of the Maximum Energy window has slightly higher sidelobes immediately adjacent to the mainlobe, but lower sidelobes thereafter. Additionally, there is slightly more headroom between the impulse response and the sidelobe limit specification for the Maximum Energy window.

We also note that the interval width  $X$  over which the impulse response of the Maximum Energy window was optimized (to maximize its energy content) corresponds to 2.24 times the half-power width (from an abscissa value of zero to 1.12 in Fig. 6). Some additional parameters are compared in the following table.

	Taylor -35 dB sidelobes $n_{\text{bar}} = 4$	Maximum Energy $c = 4.1432$
Required bandwidth extension to maintain -3 dB width to one unit	1.18	1.18
Impulse response -18 dB width relative to -3 dB width	2.21	2.18
Impulse response first null position relative to -3 dB width	1.41	1.34
Signal to Noise Ratio (SNR) gain relative to no windowing	-0.91 dB	-0.89 dB
Peak sidelobe level relative to mainlobe peak	-35.2 dB	-29.2 dB
Integrated sidelobe ratio (relative energy beyond 1.12 units from mainlobe peak)	-24.1 dB	-25.0 dB

This data suggests that the Taylor window exhibits very nearly optimum performance from a maximum energy standpoint, and is an excellent choice for Synthetic Aperture Radar processing. An image processed with the Maximum Energy window is shown in Fig. 7.



Fig. 7 Synthetic Aperture Radar image of Sandia National Laboratories robotic test range at 4-inch resolution, processed with a Maximum Energy window.

### 3 Maximum Energy Windowing With Stop-Bands

The solution to the problem of windowing with stop-bands requires the solution to a new eigenvalue problem. In this case, we want to maximize an energy ratio given by Eq. (7) with  $f(x)$  given by

$$f(x) = \frac{1}{2p} \int_B F(\mathbf{w}) e^{i\mathbf{w}x} d\mathbf{w}, \quad (16)$$

where  $B$  is the domain that defines the range of integration. Generally,  $B$  can be represented as a sum (union) of closed intervals. Equivalently, we can write Eq. (16) as

$$f(x) = \frac{1}{2p} \int_{-\infty}^{\infty} S(\mathbf{w}) F(\mathbf{w}) e^{i\mathbf{w}x} d\mathbf{w}, \quad (17)$$

where  $S(\mathbf{w}) = 1, 0$  is an indicator function defining the support of the range of integration. It is assumed that  $S(\mathbf{w}) = 0, |\mathbf{w}| > \Omega$ , where  $\Omega$  defines the spectral width without notches.  $S(\mathbf{w})$  can generally be written as a sum of rect functions. A representative plot of  $S(\mathbf{w})$  is shown in Fig. 8. Note that the stop-band need not be centered and its width and position are design parameters that affect the solution.

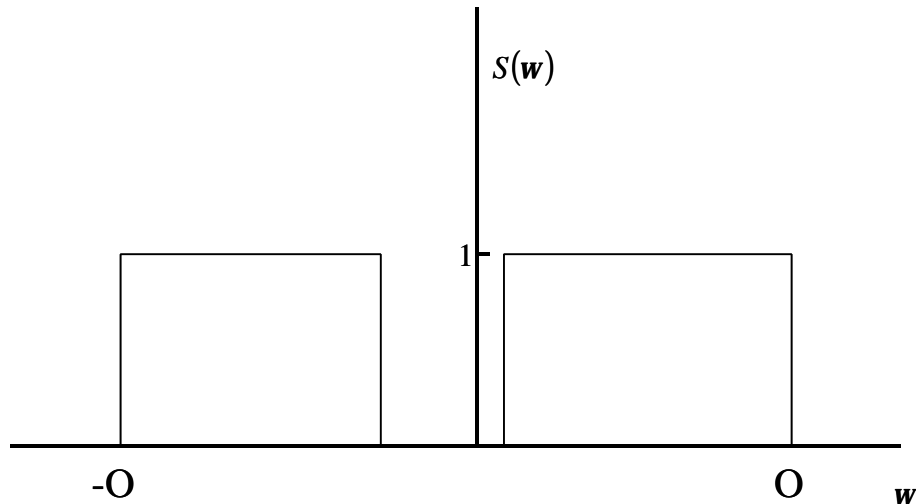


Fig. 8 Representative spectrum with stop band.

Substituting Eq. (16) into Eq. (7) gives

$$E = \frac{\int_{-X/2}^{X/2} \int_B \int_B F^*(\mathbf{w})F(\mathbf{s}) e^{i(\mathbf{s}-\mathbf{w})x} d\mathbf{s} d\mathbf{w} dx}{\int_{-\infty}^{\infty} \int_B \int_B F^*(\mathbf{w})F(\mathbf{s}) e^{i(\mathbf{s}-\mathbf{w})x} d\mathbf{s} d\mathbf{w} dx}. \quad (18)$$

We can perform the integration in the numerator with respect to  $x$  to obtain

$$D = \int_{-X/2}^{X/2} e^{i(\mathbf{s}-\mathbf{w})x} dx = \frac{2 \sin(\mathbf{s} - \mathbf{w})X/2}{\mathbf{s} - \mathbf{w}} = \frac{X}{\mathbf{p}} \operatorname{sinc} \left[ \frac{(\mathbf{s} - \mathbf{w})X}{2\mathbf{p}} \right]. \quad (19)$$

Also, from the last relation in Eq. (19) we can see that  $D$  approaches a delta function as  $X$  approaches infinity. That is,

$$\lim_{X/2 \rightarrow \infty} D = 2\mathbf{p}d(\mathbf{s} - \mathbf{w}). \quad (20)$$

Equation (19) and (20) can be applied respectively to the numerator and denominator of Eq. (18) to obtain

$$E = \frac{\int_B \int_B F^*(\mathbf{w})F(\mathbf{s}) \frac{\sin(\mathbf{w} - \mathbf{s})X/2}{\mathbf{w} - \mathbf{s}} d\mathbf{s} d\mathbf{w}}{\mathbf{p} \int_B F^*(\mathbf{w})F(\mathbf{w}) d\mathbf{w}}. \quad (21)$$

This result can be, equivalently, written as

$$E = \frac{(AF, F)_B}{\|F\|_B^2}, \quad (22)$$

where the operator  $A$  is defined by

$$AF(\mathbf{w}) = \frac{1}{\mathbf{p}} \int_B \frac{\sin(\mathbf{w} - \mathbf{s})X/2}{\mathbf{w} - \mathbf{s}} F(\mathbf{s}) d\mathbf{s}. \quad (23)$$

Since  $A$  is a (linear) compact, self-adjoint, positive definite operator on  $I$ , we know that a unique solution exists, and the maximum is given by the largest eigenvalue of the equation

$$A\mathbf{y} = I\mathbf{y}, \quad (24)$$

and the windowing function is given by the corresponding eigenfunction. Of course, this solution gives the result of Eq. (10) when there is no stop-band. The above development closely follows the formulation for the antenna problem in Harger.<sup>11</sup>

### 3.1 Solution for the Centered Stop-Bands

In the following we develop solutions to Eq. (23) for the case of a stop-band that is centered in the system spectral band. That is, the system the bandpass consists of the following interval,

$$\mathbf{w} \in B \quad \text{iff} \quad \mathbf{e}\Omega \leq |\mathbf{w}| \leq \Omega. \quad (25)$$

In this case our integral equation, Eq. (24) can be written as

$$\frac{1}{P} \int_B \Phi(\mathbf{a}) \frac{\sin(c(\mathbf{w}-\mathbf{a}))X/2}{\mathbf{w}-\mathbf{a}} d\mathbf{a} = I\Phi(\mathbf{w}), \quad (26)$$

where

$$c = \Omega X/2, \quad (27)$$

and

$$\mathbf{w} \in B \quad \text{iff} \quad \mathbf{e} \leq |\mathbf{w}| \leq 1. \quad (28)$$

This integral equation is symmetric with respect to reflections about the axis  $\mathbf{w} = 0$ . This implies that if  $\Phi(\mathbf{w})$  is an eigenfunction of this equation with eigenvalue  $I$

then  $\Phi(-\mathbf{w})$  is also an eigenvalue of this equation with eigenvalue  $I$ . If  $I$  is a simple eigenvalue, then we must have

$$\Phi(-\mathbf{w}) = m\Phi(\mathbf{w}). \quad (29)$$

Applying this inversion again we see that we must have

$$m^2 = 1, \quad (30)$$

and hence

$$m = \pm 1. \quad (31)$$

This shows that any eigenfunction associated with a simple eigenvalue must either be symmetric or anti-symmetric. Symmetric eigenfunctions satisfy

$$\Phi(\mathbf{w}) = \Phi(-\mathbf{w}), \quad (32)$$

and anti-symmetric eigenfunctions satisfy

$$\Phi(\mathbf{w}) = -\Phi(-\mathbf{w}). \quad (33)$$

Since our basic eigenvalue problem is real and self-adjoint, we know that the eigenfunctions  $\Phi(\mathbf{w})$  must be real. It follows that the transform  $f(x)$  of a symmetric eigenfunction will be real and even, and the transform of an anti-symmetric eigenfunction will be imaginary and odd.

We have written a Tchebychev collocation program to numerically obtain the eigenvalues of this integral equation. For  $\epsilon = 0$  we have the integral equation for the case with no gap. In this case the largest eigenvalue has a symmetric eigenfunction. Numerical calculations show that there is a critical value of  $\epsilon$  where the eigenfunction associated with the largest eigenvalue is antisymmetric. Fig. 9 shows a plot of the largest symmetric eigenvalue and the largest anti-symmetric eigenvalue for the case with  $c = 4$ .

We see that for  $\epsilon$  between about .05 and .55 the largest eigenvalue has an anti-symmetric eigenfunction.

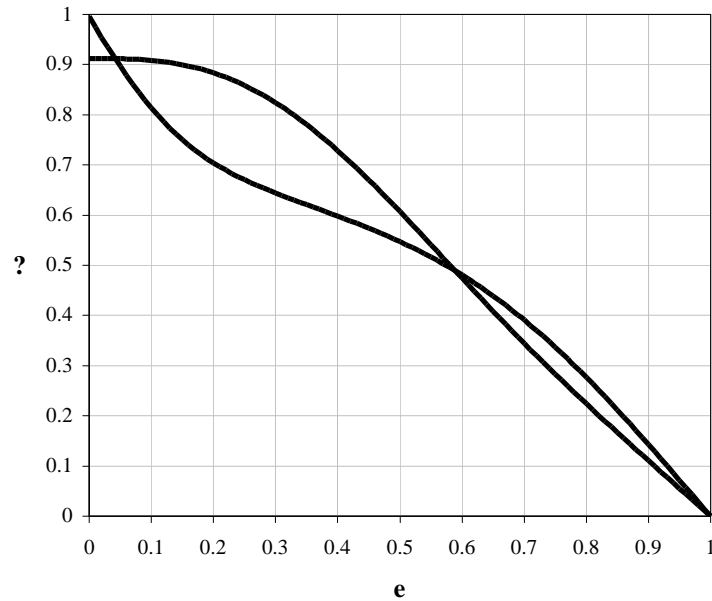
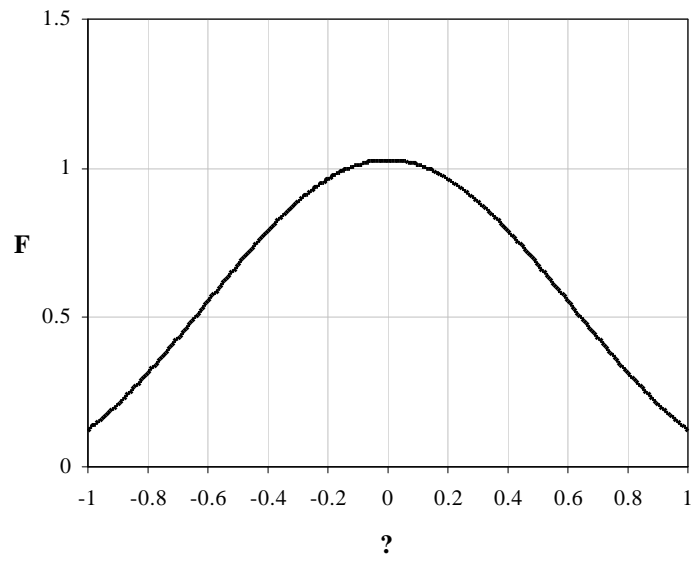


Fig. 9 A plot of the largest symmetric eigenvalue, and the largest antisymmetric eigenvalue as a function of the gap  $\epsilon$  for  $c = 4$ .

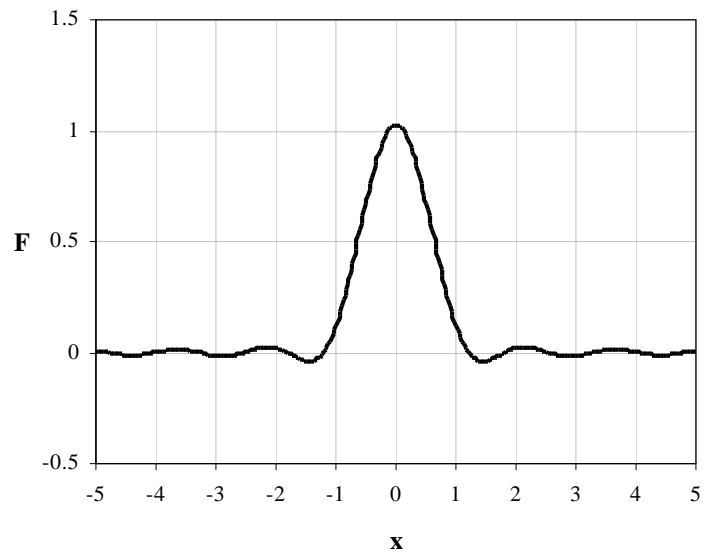
When the largest eigenvalue has an anti-symmetric eigenfunction, this means that the bandlimited function  $f(x)$  that has the most energy in the interval  $|x| \leq 1$  has no energy at  $x = 0$ , and is antisymmetric. Fig. 10 through Fig. 15 give examples of the largest symmetric and anti-symmetric modes for  $c = 4$ , and  $\epsilon = 0, .1$  and  $.2$ .

Unfortunately, at this point we effectively have a solution to windowing problem for a notched spectrum. The result is that the maximum energy criterion does not give a good solution to the windowing with respect to peak-to-sidelobe ratio. This is illustrated dramatically in Fig. 9. A good solution for a 35 dB peak to side-lobe-ratio would require an eigenvalue with something on the order of three nines after the decimal

point. It can be seen from Fig. 9 that a good solution would be obtained for extremely narrow notches. This is further illustrated in Fig. 10 through Fig. 15, where it is clear that a classical SAR impulse response is not obtained for significant notches in the spectrum. In the next section we address this result from the standpoint of perturbation theory. We also generalize the argument that the presence of notches in the system spectrum prohibits large peak-to-sidelobe ratios.

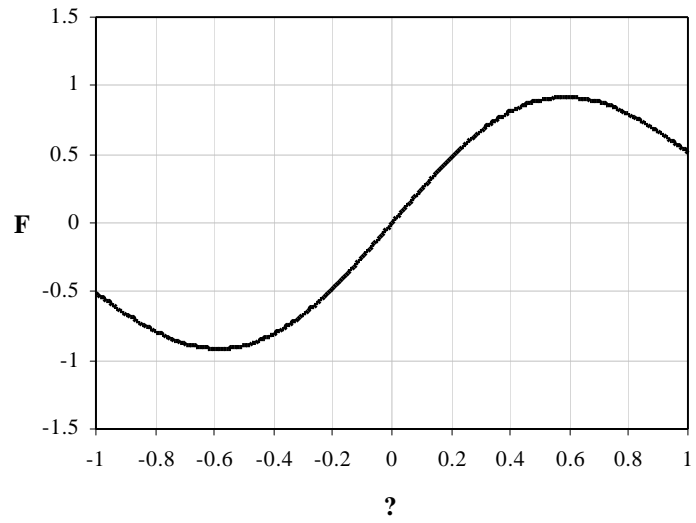


(a)

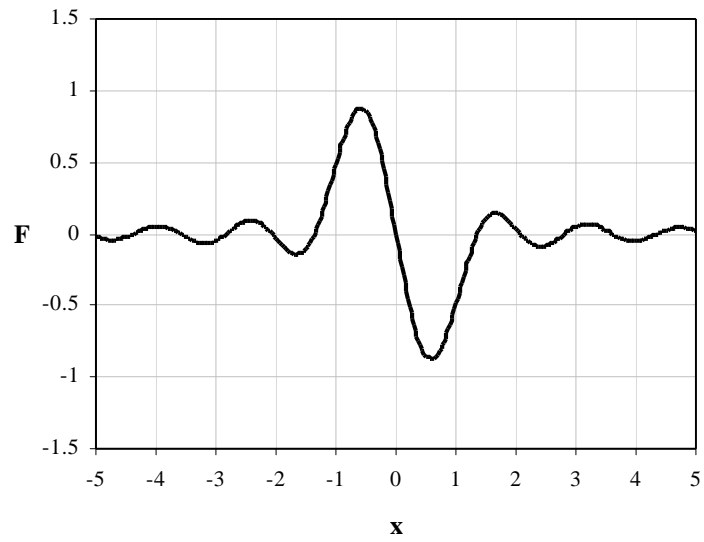


(b)

Fig. 10 Plots of (a) the eigenfunction  $\Phi(\mathbf{w})$  and (b) the transform  $f(x)$  for  $\mathbf{e} = 0$  and  $c = 4$ . This is the even eigenfunction associated with the largest eigenvalue.

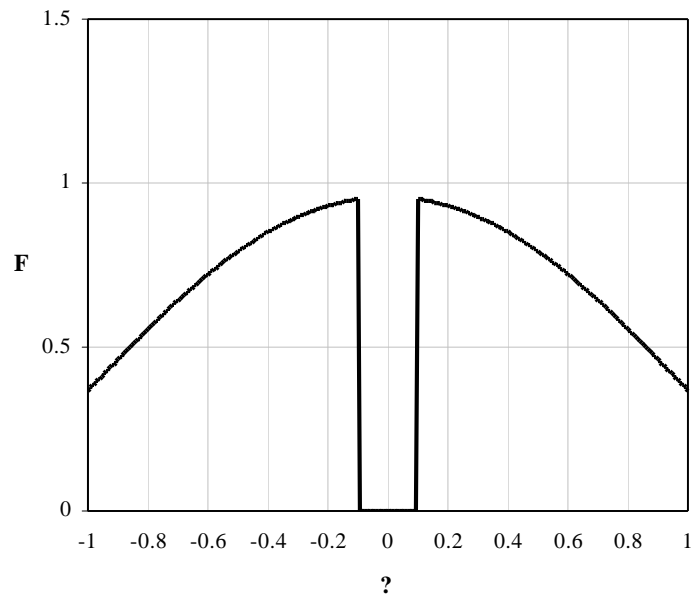


(a)

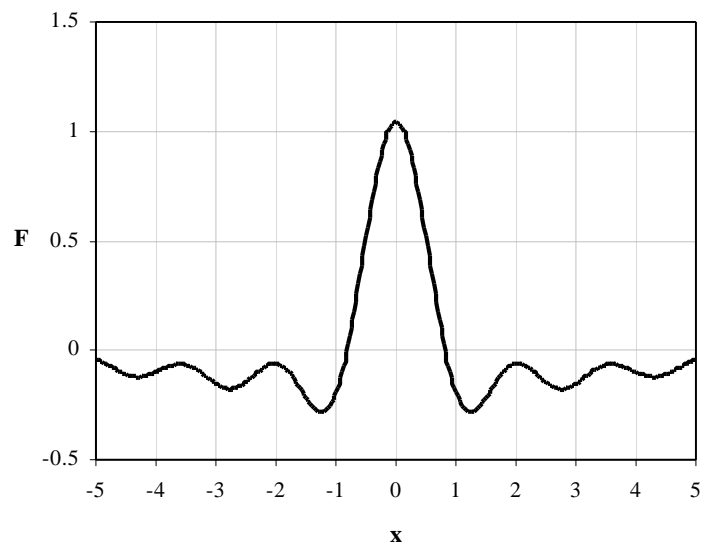


(b)

Fig. 11 Plots of (a) the eigenfunction  $\Phi(\mathbf{w})$  and (b) the transform  $f(x)$  for  $\mathbf{e} = 0$  and  $c = 4$ . This is the odd eigenfunction associated with the largest eigenvalue.

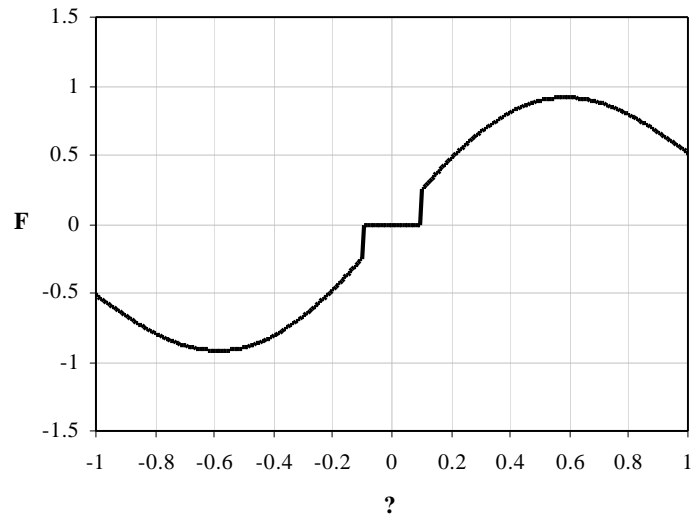


(a)

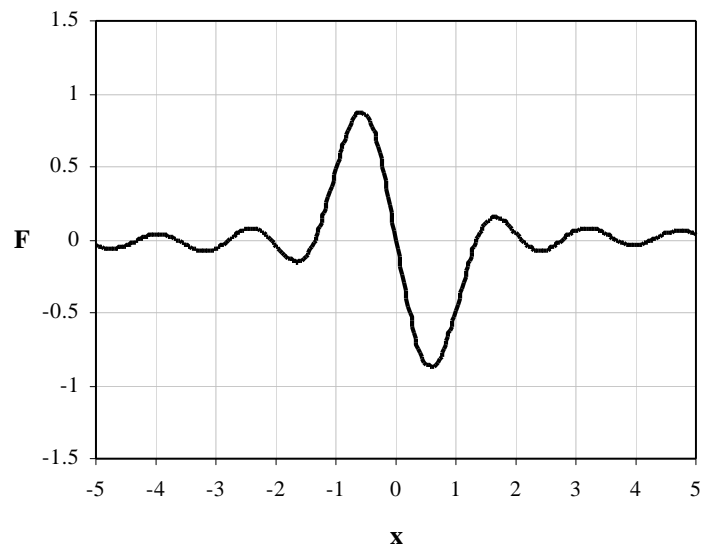


(b)

Fig. 12 Plots of (a) the eigenfunction  $\Phi(\mathbf{w})$  and (b) the transform  $f(x)$  for  $\epsilon = .1$  and  $c = 4$ . This is the even eigenfunction associated with the largest eigenvalue.

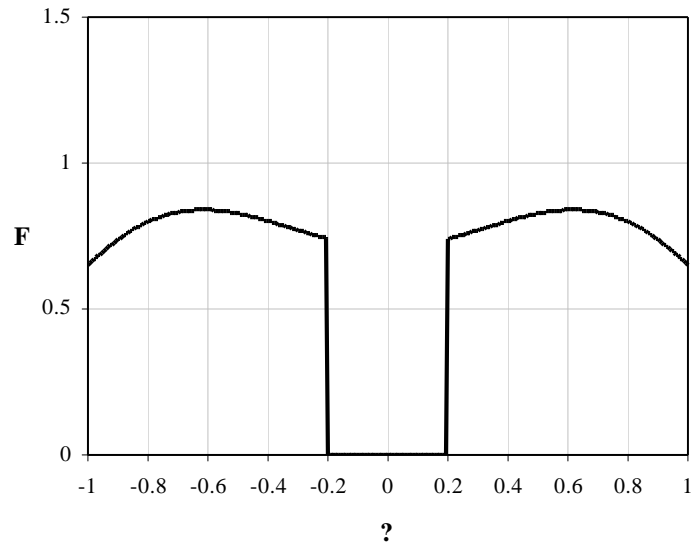


(a)

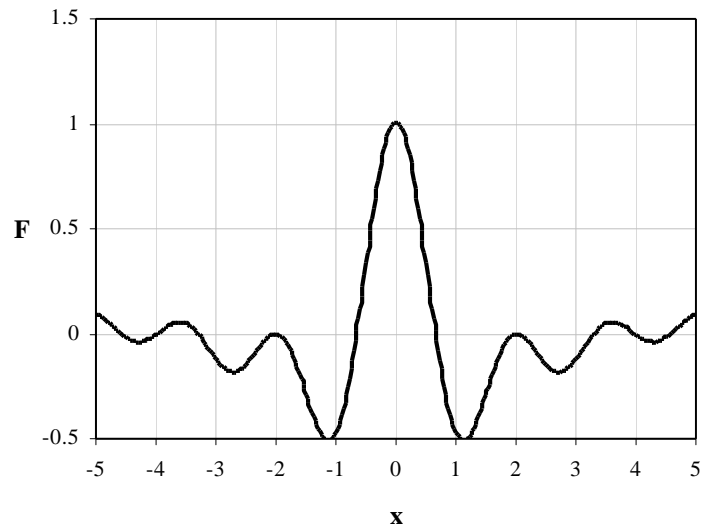


(b)

Fig. 13 Plots of (a) the eigenfunction  $\Phi(\mathbf{w})$  and (b) the transform  $f(x)$  for  $\epsilon = .1$  and  $c = 4$ . This is the odd eigenfunction associated with the largest eigenvalue.

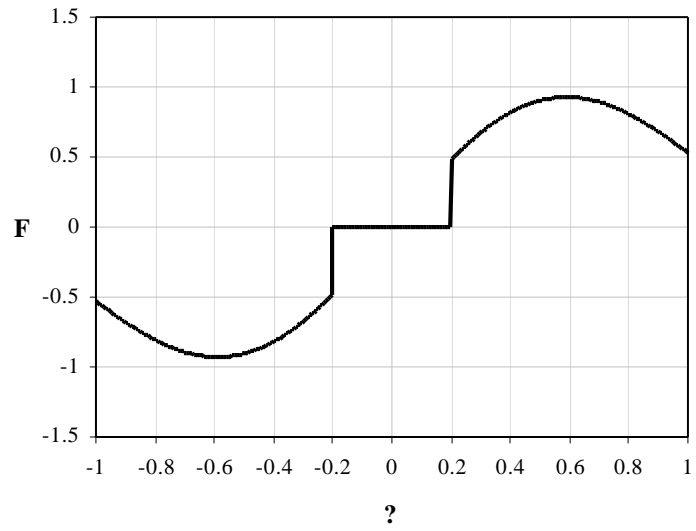


(a)

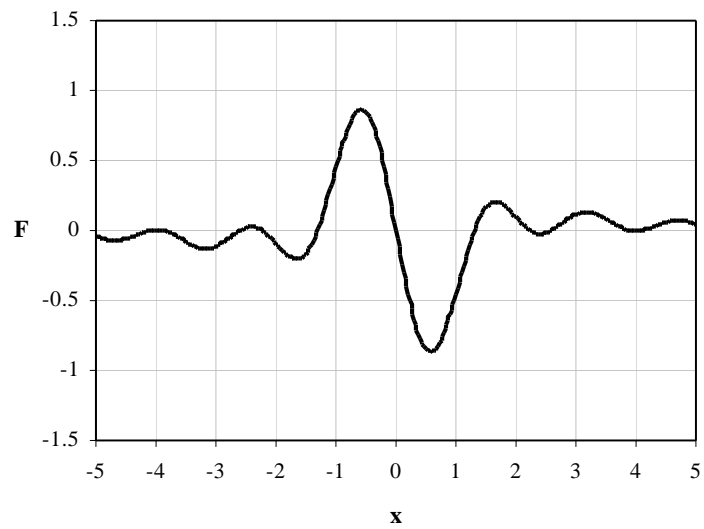


(b)

Fig. 14 Plots of (a) the eigenfunction  $\Phi(\mathbf{w})$  and (b) the transform  $f(x)$  for  $\epsilon = .2$  and  $c = 4$ . This is the even eigenfunction associated with the largest eigenvalue.



(a)



(b)

Fig. 15 Plots of (a) the eigenfunction  $\Phi(\mathbf{w})$  and (b) the transform  $f(x)$  for  $\epsilon = .2$  and  $c = 4$ . This is the odd eigenfunction associated with the largest eigenvalue.

## 3.2 Perturbation Theory

Let  $I_0(c, \mathbf{e})$  be the largest eigenvalue as a function of  $c$  and  $\mathbf{e}$ . When  $\mathbf{e}$  is zero, this is identical to the eigenfunction with no notch. If  $c$  is large, and  $\mathbf{e}$  is big enough, then  $I$  will be approximately the eigenvalue that we would get if we did our optimization by including only one of the pieces of the spectrum. This would be equivalent to doing the optimization with  $c = \hat{c}$  where  $\hat{c} = (c - \mathbf{e})/2$ .

When  $c$  is large, a very small value of  $\mathbf{e}$  will change  $I$  from the value with the full bandwidth to that having only half the bandwidth. We now present an argument from the perturbation theory of eigenvalues that makes this calculation explicit.

Suppose we have a linear self-adjoint operator

$$L = L_0 + \mathbf{d}L \quad (34)$$

where  $\mathbf{d}L$  is a small perturbation to the operator  $L_0$ . We suppose that the operator  $L_0$  has an eigenvalue  $I_0$  that goes to

$$I = I_0 + \mathbf{d}I \quad (35)$$

when we add the perturbation  $\mathbf{d}L$  to  $L_0$ . Let  $\Phi_0(\mathbf{w})$  be an eigenfunction associated with the operator  $L_0$ , and the eigenvalue  $I_0$ . The perturbation theory of eigenvalues shows that the perturbation  $\mathbf{d}I$  to the eigenvalue is given by

$$\mathbf{d}I = \frac{(\Phi, \mathbf{d}L \Phi)}{(\Phi, \Phi)} \quad (36)$$

In our particular case, we consider the operator  $L_0$  to be

$$L_0 \Phi = \int_{-1}^1 \text{Sinc}(c(\mathbf{w} - \mathbf{a})) \Phi(\mathbf{a}) d\mathbf{a} , \quad (37)$$

and the operator  $dL$  to be

$$dL\Phi = \int_{-e}^e \text{Sinc}(c(\mathbf{w} - \mathbf{a})) \Phi(\mathbf{a}) d\mathbf{a} . \quad (39)$$

If  $\Phi$  is a normalized eigenfunction, the perturbation theory of eigenvalues implies that

$$dI = \int_{-1}^1 \int_{-e}^e \text{Sinc}(c(\mathbf{w} - \mathbf{a})) \Phi(\mathbf{a}) \Phi(\mathbf{w}) d\mathbf{a} d\mathbf{w} . \quad (40)$$

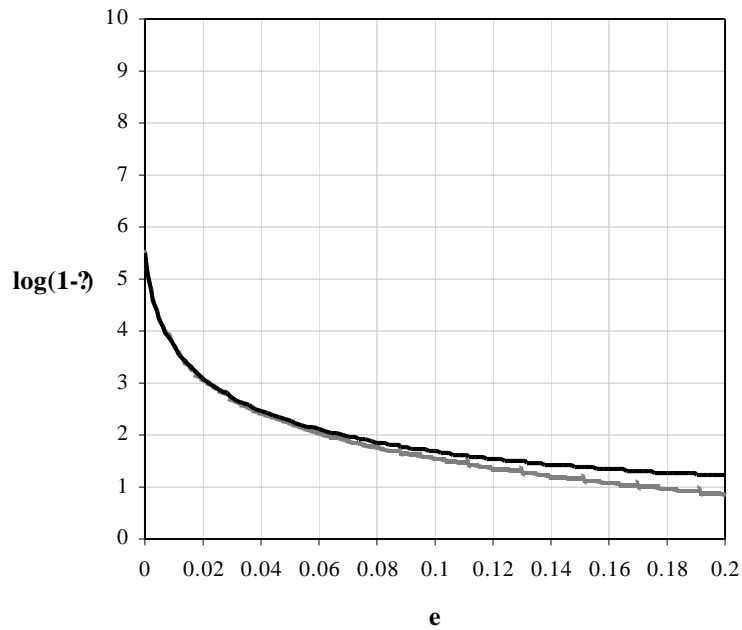
If we reverse the roles of the integrals, and integrate with respect to  $c$  first we get

$$dI = -I_0 \int_{-e}^e \Phi^2(\mathbf{a}) d\mathbf{a} \approx -2I_0 e \Phi^2(0) . \quad (41)$$

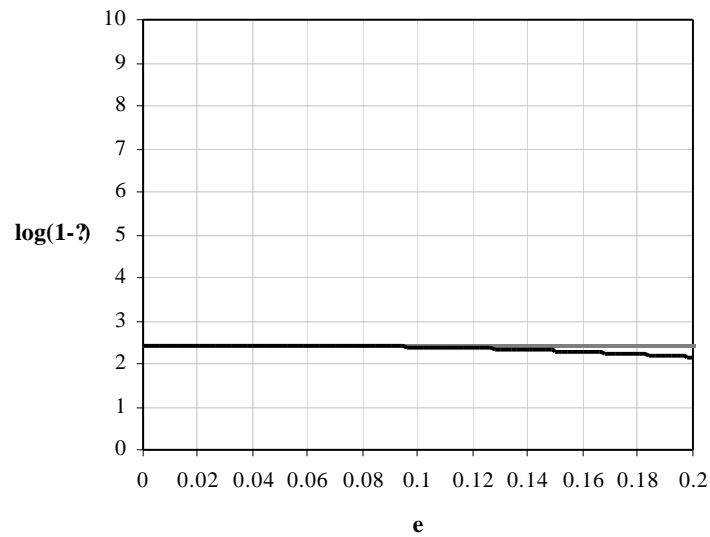
This result has some interesting consequences. A small perturbation has very little effect on the eigenvalues associated with anti-symmetric eigenfunctions.

For large values of  $c$ , the largest eigenvalue is very close to unity. The perturbations to largest eigenvalue will very quickly move the eigenvalue away from unity.

Fig. 16 shows the comparison between the perturbation theory of eigenvalues and the exact numerical results for  $c = 4$ . We see that perturbation theory gives excellent results for both the symmetric and anti-symmetric eigenfunctions up to about  $e = .05$ . This is a small value of  $e$ , but we see that for the symmetric mode a lot of change takes place in this interval. The perturbation theory gives quite respectable results out to  $e = .2$ .



(a)



(b)

Fig. 16 A comparison between perturbation theory and the exact numerical results (dark line) of  $1-I$ : (a) The largest symmetric eigenvalue, (b) The largest anti-symmetric eigenvalue. These results are for  $c = 4$ .

We can readily extend the result in Eq. (40) to include to the case when the notch is not centered. The result is,

$$dI \approx -2I_0 \mathbf{e} \Phi^2(\mathbf{e}_0), \quad (42)$$

where  $\mathbf{e}_0$  is the location of the center of the notch. The major result is that although the decrease in  $I$  is a rapid function of  $\mathbf{e}$  the decrease goes to zero (or a minimum) as  $\mathbf{e}_0$  approaches a minimum or null of  $\Phi^2$ . This implies that moving the notch to the edge of the bandpass of the system would result in minimum impact on the system, which is what one would expect. However, putting the notch at the end of the spectrum is not an interesting problem.

Perturbation theory also gives a simple expression for the inverse Fourier transform  $\mathbf{f}(x)$  of the eigenfunctions. The inverse Fourier transform is given by

$$\mathbf{f}(x) = \frac{1}{2\mathbf{p}} \int_B \Phi(\mathbf{w}) e^{-i\mathbf{w}x} d\mathbf{x}. \quad (43)$$

When  $\mathbf{e}$  is small, the eigenfunctions  $\Phi(\mathbf{w})$  are close to those for the contiguous-spectrum or unnotched case. In this case we can write

$$\mathbf{f}(x) = \frac{1}{2\mathbf{p}} \int_{-1}^1 \Phi(\mathbf{w}) e^{-i\mathbf{w}x} d\mathbf{x} - \frac{1}{2\mathbf{p}} \int_{-e}^e \Phi(\mathbf{w}) e^{-i\mathbf{w}x} d\mathbf{x}. \quad (44)$$

Since  $\mathbf{e}$  is small, we can approximate this as

$$\mathbf{f}(x) \approx \mathbf{f}_0(x) - \frac{\Phi(0)\mathbf{e}}{\mathbf{p}} \text{sinc}(e\mathbf{x}/\mathbf{p}), \quad (45)$$

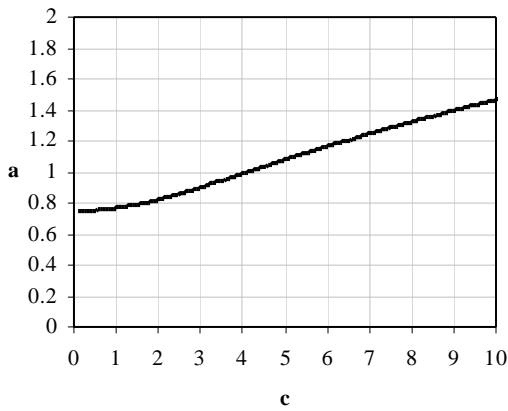
where  $\mathbf{f}_0(x)$  is the function for the unnotched case. Thus, for small  $\mathbf{e}$  we have the windowed function minus a small sinc function. This sinc function is much wider than  $\mathbf{f}_0(x)$ . Thus main lobe of the sinc function subtracts relatively flat (constant) plateau from  $\mathbf{f}_0(x)$ . The effect is to significantly alter the sidelobe height in an adverse way while having a small effect on the resolution.

### 3.3 The Iteration

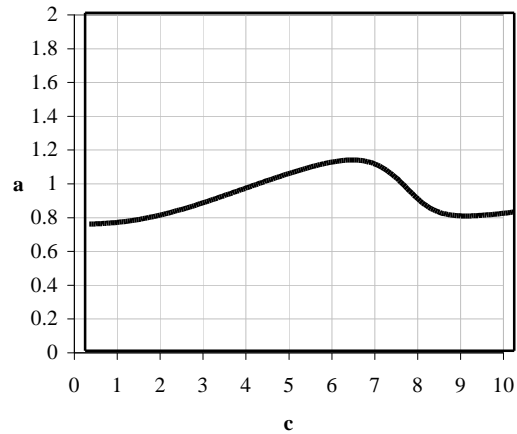
The iteration described in Appendix B can be put in the following form. Let  $x(c)$  be the half power point of the function  $f(x)$  that maximizes the energy inside the interval  $(-c/2, c/2)$  subject to the constraint that its Fourier transform is bandlimited to the region  $e < |w| < 1$ . To avoid confusion we will limit ourselves to symmetric functions. As in the case with no notch we try to find a value of  $c$  that allows us to make a fair comparison to the Taylor window. In order to do this we choose the value of  $c$  such that  $a(c)=1$ , where

$$a(c) = \frac{2cx(c)}{3.71}. \quad (46)$$

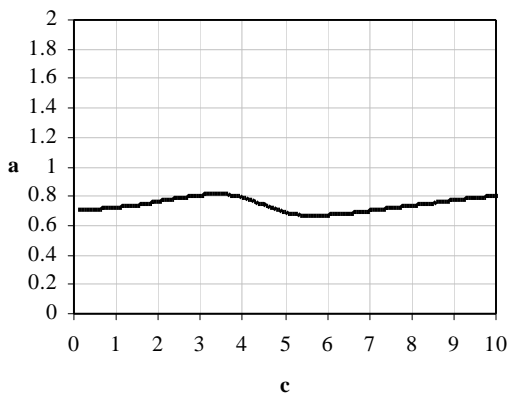
Fig. 17 shows a plot of the function  $a(c)$  for different values of  $e$ . We see that if  $e$  is large enough, then the function never is bigger than one, and there is no solution to  $a(c)=1$ . Note that in the cases shown in Fig. 17 where there is a solution, there are two solutions. We see that extremely small values of  $e$  dramatically change the appearance of the function  $a(c)$



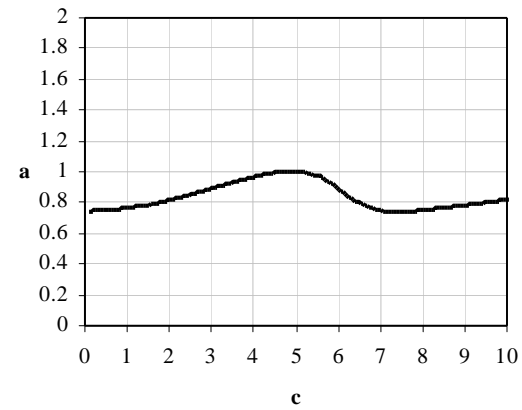
(a)



(b)



(c)



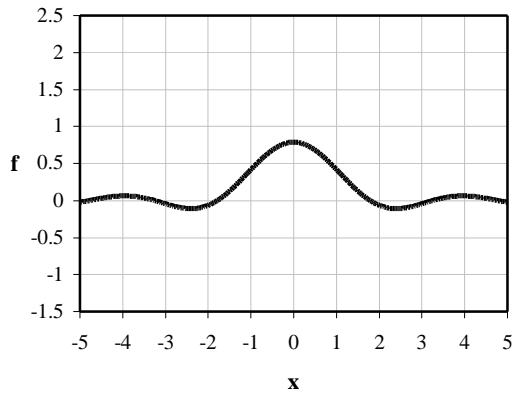
(d)

Fig. 17 The function  $\mathbf{a}(c)$  for; (a)  $\mathbf{e} = 0$ , (b)  $\mathbf{e} = .001$ , (c)  $\mathbf{e} = .01$ , (d)  $\mathbf{e} = .1$ .

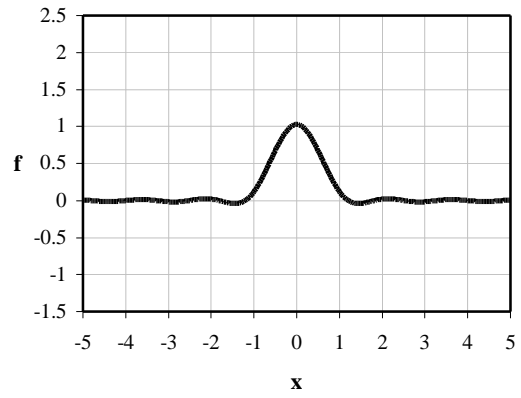
This extreme sensitivity to  $\mathbf{e}$  is consistent with our results from perturbation theory that show that very small values of  $\mathbf{e}$  change the value of  $\mathbf{I}$  significantly. For a given value of  $c$ , there is a crudely defined value  $\mathbf{e}_c(c)$  where the eigenfunctions cease to look like the eigenfunctions with  $\mathbf{e} = 0$ . Beyond this value of  $c$  the eigenfunctions are more like those we would get by only including one of our intervals, but then symmetrizing it to include both intervals. This value of  $\mathbf{e}_c(c)$  is very small when  $c$  is

large. The curves for  $\mathbf{a}(c, \mathbf{e})$  will look much like the curve  $\mathbf{e}(c, 0)$  up until we reach a value of  $c$  such that  $\mathbf{e}_c(c) > 0$ .

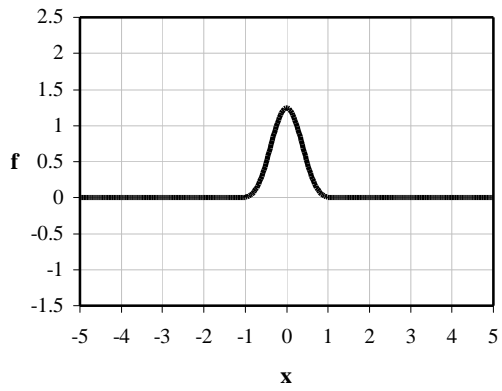
Fig. 18 and Fig. 19 help explain the strange appearance of the curve  $\mathbf{a}(c)$  for nonzero values of  $\mathbf{e}$ . In these figures we show the functions  $\mathbf{f}(x)$  for different values of  $c$ , and for  $\mathbf{e} = 0$ , and  $\mathbf{e} = .01$ . We see that for small values of  $c$  the functions  $\mathbf{f}(x)$  with  $\mathbf{e} = 0$ , and  $\mathbf{e} = .01$  agree with each other. Once  $c$  gets to be bigger than a critical value they differ dramatically.



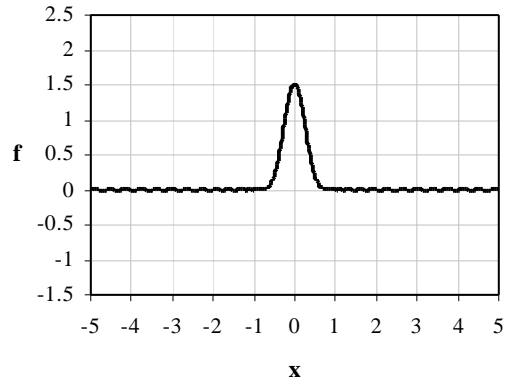
(a)



(b)



(c)



(d)

Fig. 18 The functions  $f(x)$  for  $e = 0$  and (a)  $c = 2$ , (b)  $c = 4$ , (c)  $c = 8$ , (d)  $c = 16$ .

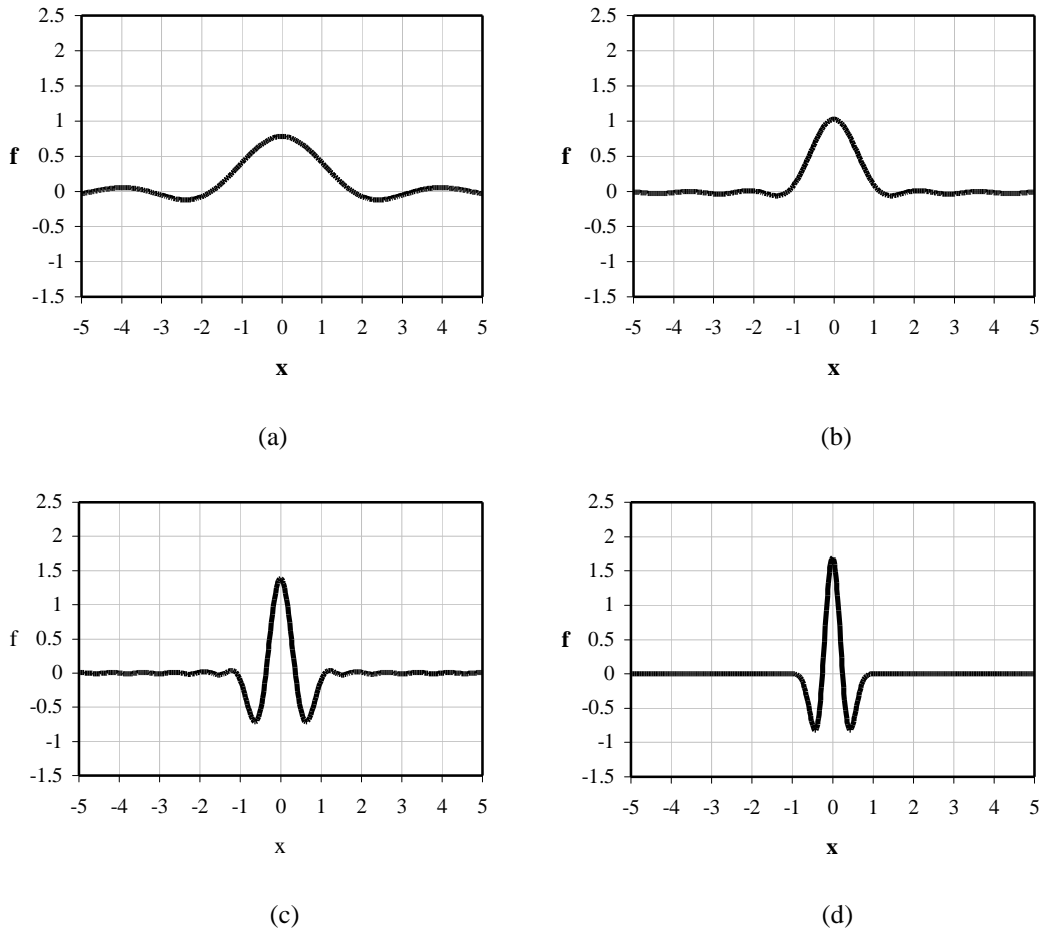


Fig. 19 The functions  $f(x)$  for  $\epsilon = .01$  and (a)  $c = 2$ , (b)  $c = 4$ , (c)  $c = 8$ , (d)  $c = 16$ .

The eigenfunctions of our problem must be either symmetric or anti-symmetric. For a given value of  $\epsilon > 0$ , if  $c$  is big enough, then the functions that minimizes the energy is very nearly equal to the function we would get by doing this optimization problem if we used only one of the humps. Given that all eigenfunctions must be either symmetric or antis-symmetric, the only way we can achieve this is if we have two modes that have almost identical eigenvalues, one of them being symmetric and the other anti-symmetric. By combining these modes we can get functions that exist on one hump or the other. If we transform the symmetric mode we get a real valued functions  $f(x)$ , if we

transform the anti-symmetric, we get an imaginary functions  $\mathbf{y}(x)$ . The function  $\mathbf{f}^2 + \mathbf{y}^2$  should be very close to the function we would get if we solved our optimization problem with a bandwidth of  $c/2$ .

### 3.4 Alternatives to Windowing for Sidelobe Control

As shown, the maximum energy criterion analysis indicates that windowing is unlikely to produce satisfactory peak to sidelobe ratios for significant spectral gaps. This begs the question “What are the alternatives to push down sidelobes?” The purpose is, of course, to render a more aesthetic image, and not necessarily a more accurate one. This suggests employing nonlinear and perhaps heuristic image processing techniques, in the vein of superresolution, to essentially fill in the missing spectrum with “nice” data. Such techniques can be quite effective in presenting an aesthetically improved image, but can also often yield unexpected results and introduce their own artifacts, which may ultimately render a less accurate image of the target scene.

As an example, one such technique is the CLEAN<sup>12,13</sup> algorithm first developed for astronomical imaging, and later adapted to microwave imaging by Tsao and Steinberg.<sup>14</sup> A similar algorithm used by Wahl, et al., resulted in substantial improvement to the visual appeal of fine-resolution L-band and S-band SAR imagery.<sup>15</sup> These techniques essentially identify and then subtract objectionable target responses from an image and replace them with more ideal responses. Other techniques often employ a similar presumption of point targets.<sup>16,17,18</sup> A more comprehensive inventory of such techniques is beyond the scope of this paper.

## 4 Least Squares Reconstruction

The windowing of SAR data prior to transformation into an image is a well established technique. The primary impetus for windowing is to mitigate deleterious effect in the visual character of the image associated with the sidelobes of the system impulse response. However, it can be argued that the minimum-mean-squared-error imaging of the target is achieved with no windowing at all (rectangular or boxcar window). The purpose here is not to argue against (or for) windowing, but to point out a property of the image construction process that may have general applicability to image processing or pattern recognition.

The basic argument is as follows. It is well known that when a function is expanded in terms of an orthonormal set of functions  $\mathbf{f}_i(x)$ , the best least-squares fit is obtained using the Fourier (expansion) coefficients  $a_i$ .<sup>19</sup> That is, for a least squares fit with orthogonal functions the  $a_i$  are determined independently and if we decide to change the number of the functions,  $\mathbf{f}_i(x)$ , that we use in the expansion we do not need to redetermine the expansion coefficients. Further, since the SAR data is band-limited, the image inversion problem consists in determining the expansion coefficients in an expansion of the form,

$$s(x) = \sum_0^N a_i \mathbf{f}_i(x), \quad (47)$$

where  $\mathbf{f}_i(x)$  normalized prolate spheroidal wave functions and  $N = \Omega X / \mathbf{p}$  obtained from superresolution considerations.<sup>8,20</sup> Windowing the band-limited SAR data would result in different expansion coefficients than the inversion Fourier coefficient given in

Eq. (47) resulting in an inversion that is not optimal in a least-squares sense. The authors do not know of any reference to this simple, but surprising, result in the literature.

## 5 Summary

In this paper we have introduced a maximum energy criterion to the SAR windowing problem. This criterion provided a theoretical approach to the problem that is analytically very tractable. We applied the maximum energy criterion to the standard windowing problem and were able to show that the commonly used Taylor window exhibits characteristics very close to the optimal Maximum Energy window. Application of the maximum energy criterion to the windowing problem for SAR data with stop-bands in the spectrum showed that, except for very narrow stop-bands, the presence of stop-bands precludes obtaining large peak to sidelobe ratios by windowing. We further argue that this is a general result. We also present the simple, but surprising, result that a minimum-mean-squared-error inversion of the SAR data to form the image precludes windowing.

# Appendix A

Plots of  $y_0(c)$  for  $c = 3.0, 5.0, 6.0, 7.0, 8.0, 9.0,$  and  $10.0$  are shown in Fig. A-1 and Fig. A-2. It is interesting to observe that as  $c$  increases  $y_0$  becomes increasingly flat in the region beyond the value  $2x/X$  of the argument. This is due to the maximization of the energy in the interval  $X$ .

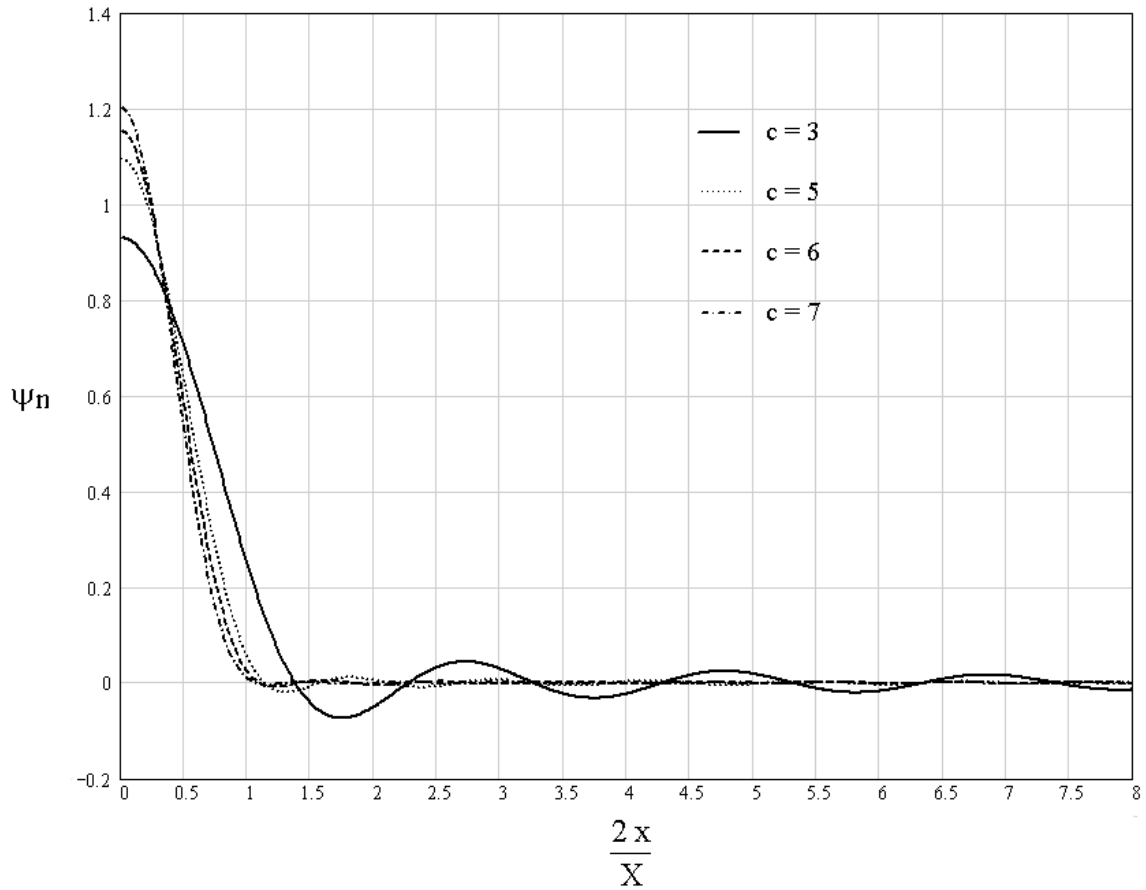


Fig. A-1 Prolate spheroidal wave functions for  $c = 3.0, 5.0, 6.0, 7.0$ .

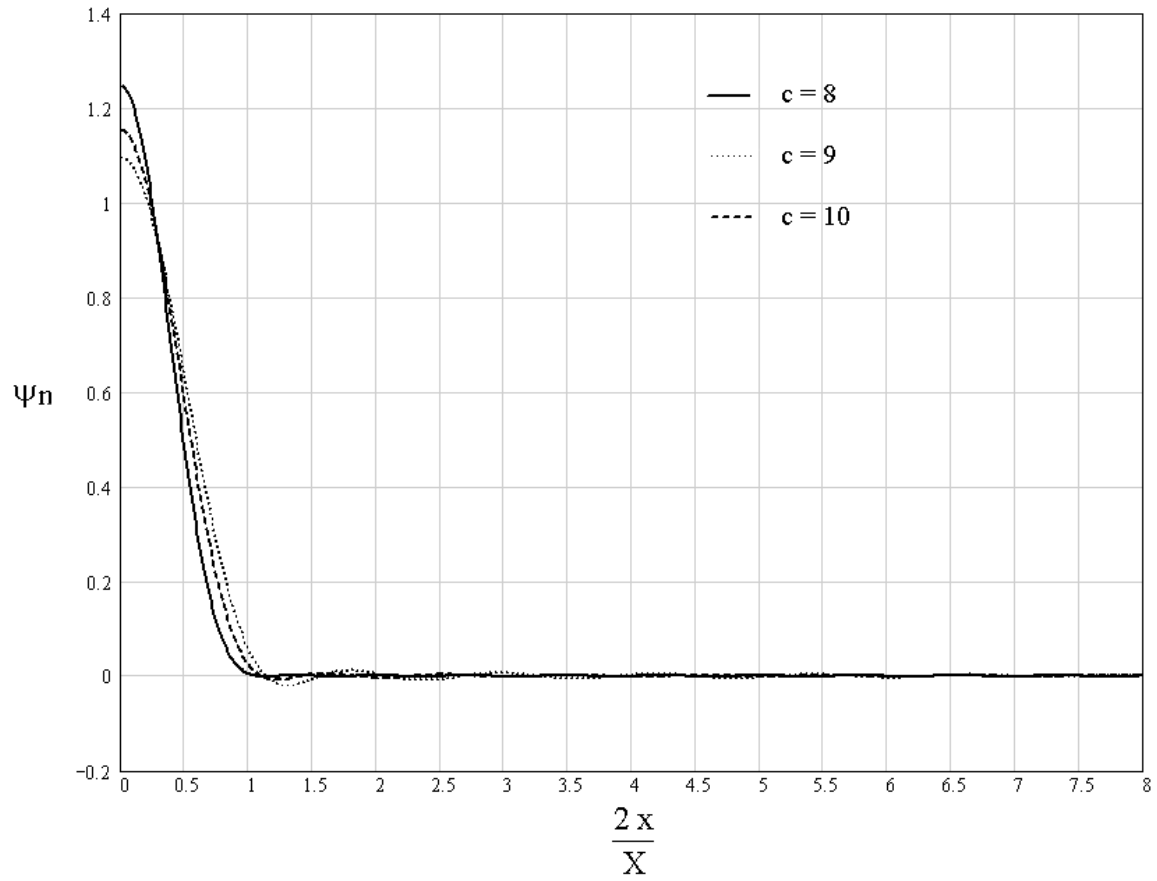


Fig. A-2 Prolate spheroidal wave functions for  $c = 8.0, 9.0, 10.0$ .

## Appendix B

The following algorithm determines the value of  $c$  for a Maximum Energy window that corresponds to the Taylor window normally used in Sandia designed SAR systems ( $-35$  dB sidelobes,  $nbar = 4$ ).

1. Pick a value of  $c$ . The value can be based on the above theory. For example, the value  $c = 4$  discussed above is a good start.
2. Calculate  $\Omega = 2cx$ , where  $x$  is obtained from the data for Fig. 4.
3. If  $\Omega = 3.71$ ,  $c$  is determined by the equation in step 2. If this relation does not hold, go to step 1.

The value  $\Omega = 3.71$  and the relation for  $\Omega$  in Step 2 are determined as follows. For this particular case we want the windowed impulse response to have a half-power point that is  $1/2$  the distance from the origin to the first zero of the corresponding sinc function. For a sinc function the distance to the first zero and the bandwidth  $\Omega$  are related by  $\Omega X = p$ , where bandwidth  $\Omega$  is defined by Eq. (6). We can arbitrarily set  $X = 1$ . For maximum energy windowing, we also require that the prolate spheroidal wave function have the same half power width. Using Fig. 4, the prolate spheroidal wave function solutions are scaled by the relation,  $\frac{X}{2} = \frac{1}{2x}$ . Substituting this result in the general relation,  $2c = \Omega X$ , we obtain  $\Omega = 2cx$ . Further, we let our bandwidth exceed that of the sinc function by a factor of 1.18, that is,  $\Omega = 1.18p = 3.71$ . The algorithm can be altered to fit a specific design problem using the above arguments.

The solution of the windowing problem for these conditions outlined above is  $c = 4.1432$ . The window function for this value of  $c$  is given in Fig. B-1. The function

in Fig. B-1 represents both the window function and the corresponding impulse response. This is a consequence of Eq. (6). The window function is obtained by scaling the function so that the unit value of the abscissa corresponds to the upper cut-off frequency of the radar spectrum (the window function is an even function). Further, for this solution,  $I = .99683$ , the peak-to-sidelobe ratio is  $R_{ps} = 29.2$  dB, and the energy ratio given by Eq. (15) is  $R = 25.0$  dB.

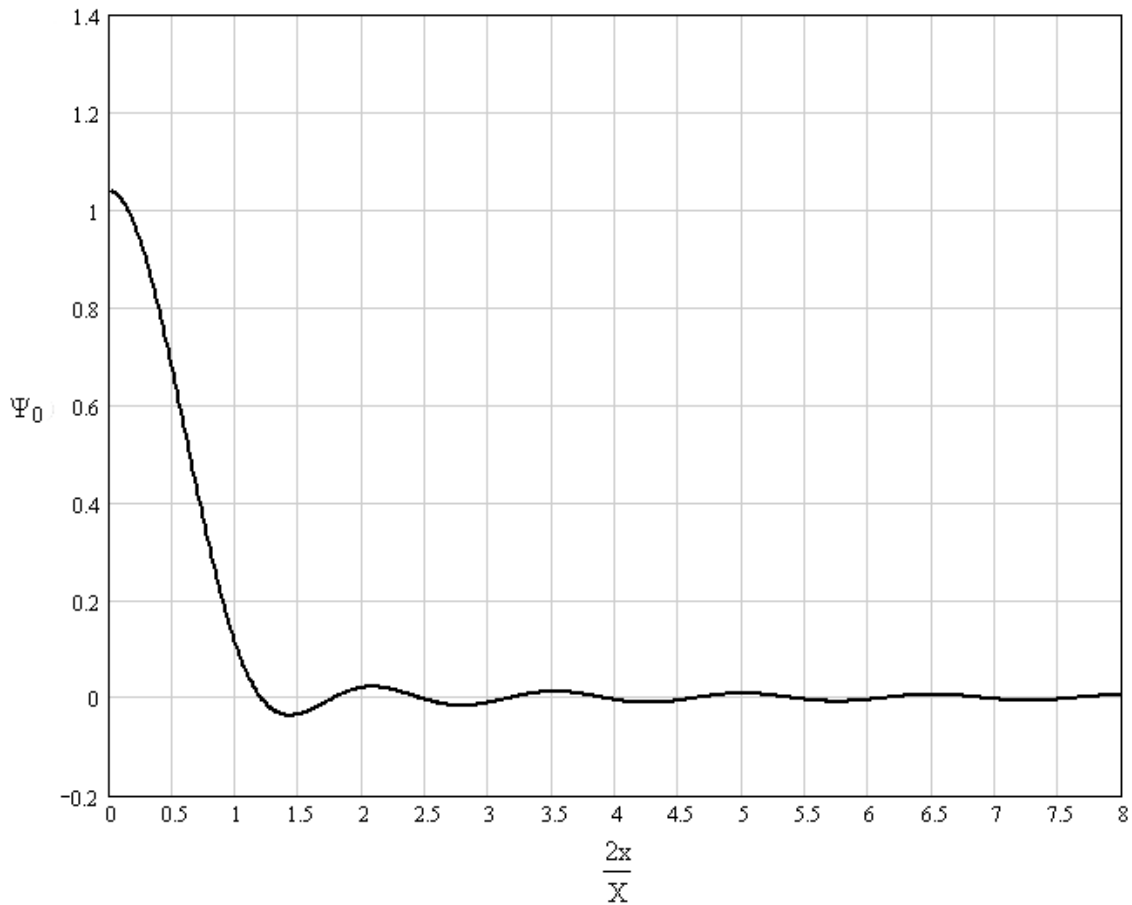


Fig. B-1 The prolate Spheroidal wave function for  $c = 4.1432$

## References

- 
- <sup>1</sup> Alan V. Oppenheim, Ronald W. Schaffer, *Digital Signal Processing*, Prentice-Hall (1975).
  - <sup>2</sup> F. M. Dickey and K. S. Shanmugam, "Optimum edge detection filter," *Applied Optics*, 16 (1), 145-148 (1977).
  - <sup>3</sup> W. H. H. J. Lunscher and M. P. Beddoes, "Optimal Edge Detector Design I: Parameter Selection and Noise Effects," *IEEE Transactions on Pattern Analysis and Machine Intelligence*, 8(2), 164-177, (1986).
  - <sup>4</sup> D. Slepian and H. O. Pollak, "Prolate Spheroidal Wave Functions, Fourier Analysis and Uncertainty – I," *The Bell System Technical Journal*, 43-63 (1961).
  - <sup>5</sup> H. J. Landau and H. O. Pollak, "Prolate Spheroidal Wave Functions, Fourier Analysis and Uncertainty – II," *The Bell System Technical Journal*, 65- 84 (1961).
  - <sup>6</sup> R. Frieden, "Evaluation, Design and Extrapolation Methods for Optical Signals, Based on Use of The Prolate Functions," Chapter VIII, *Progress In Optics, Vol. IX*, E. Wolf (Ed.), North-Holland, Amsterdam, 311 – 406, (1971).
  - <sup>7</sup> F. M. Dickey, L. A. Romero and A. W. Doerry, "Superresolution and Synthetic Aperture Radar," Sandia Report, SAND2001-1532, Sandia National Laboratories, Albuquerque, N M 87185, May (2001).
  - <sup>8</sup> F. M. Dickey, L. A. Romero, J. M. DeLaurentis, A. W. Doerry, "Superresolution, Degrees of freedom and Synthetic Aperture Radar", submitted to *Optical Engineering*.
  - <sup>9</sup> C. L. Dolph, "A Current Distribution for Broadside Arrays Which Optimizes the Relationship Between Beam Width and Side-Lobe Level", *Proceedings of the I.R.E. and Waves and Electrons*, p. 335, June (1946).
  - <sup>10</sup> T. T. Taylor, "Design of Line-Source Antenna for Narrow Beamwidth and Low Side Lobes", *IRE Transactions – Antenna and Propagation*, p. 16, January (1955).
  - <sup>11</sup> R. O. Harger, *Synthetic Aperture Radar Systems: Theory and Design*, Academic Press, New York, (1970).
  - <sup>12</sup> A. R. Thompson, J. M. Moran, and G. W. Swenson, *Interferometry and Synthesis in Radio Astronomy*, John Wiley and Sons, New York, (2001).
  - <sup>13</sup> K. Rohlfs and T. L. Wilson, *Tools of Radio Astronomy*, Springer-Verlag, Berlin, (2000).
  - <sup>14</sup> J. Tsao and B. Steinberg, "Reduction of Sidelobe and Speckle Artifacts in Microwave Imaging: The CLEAN Technique", *IEEE Transactions on Antennas and Propagation*, 36 (4), 543, April (1988).
  - <sup>15</sup> D. E. Wahl, D. A. Yocky, C. V. Jakowatz Jr., P. A. Thompson, I. A. Erteza, "Interesting Aspects of Spotlight-Mode Image Formation for an L/S-Band High-Resolution SAR ", *Proceedings of the Workshop on Synthetic Aperture Radar Technology*, Redstone Arsenal, AL, October 16 & 17 (2002).
  - <sup>16</sup> H. C. Stankwitz, M. R. Kosek, "Sparse Aperture Fill for SAR Using Super-SVA", *Proceedings of 1996 IEEE National Radar Conference*, Ann Arbor, MI, USA, 13-16 May (1996).
  - <sup>17</sup> E. G. Larsson, P. Stoica, "SAR Image Construction from Gapped Phase-History Data", *Proceedings of 2001 IEEE International Conference on Image Processing*, Thessaloniki, Greece, 3, 608-11, 7-10 Oct. (2001).

---

<sup>18</sup> E. G. Larsson, J. Li, P. Stoica, G. Liu, R. Williams, "Spectral Estimation of Gapped Data and SAR Imaging with Angular Diversity," SPIE Proceedings, 4382, *Algorithms for Synthetic Aperture Radar Imaging VIII*, 60-72, (2001).

<sup>19</sup> R. W. Hamming, *Numerical Methods for Scientists and Engineers*, McGraw-Hill Book Company, Inc., New York, (1962).

<sup>20</sup> M. Bertero and P. Boccacci, *Introduction to Inverse Problems in Imaging*, IOP Publishing, Bristol, (1998).

This page left intentionally blank.

# DISTRIBUTION

## Unlimited Release

1	MS 0509	M. W. Callahan	2300
1	MS 0519	L. M. Wells	2344
1	MS 0519	D. L. Bickel	2344
1	MS 0519	J. T. Cordaro	2344
1	MS 0519	A. W. Doerry	2344
1	MS 0519	M. S. Murray	2344
1	MS 0519	S. D. Bensonhaver	2348
1	MS 0519	T. P. Bielek	2348
1	MS 0519	S. M. Devonshire	2348
1	MS 0519	W. H. Hensley	2348
1	MS 0519	J. A. Hollowell	2348
1	MS 0519	A. L. Navarro	2348
1	MS 0519	J. W. Redel	2348
1	MS 0519	B. G. Rush	2348
1	MS 0519	G. J. Sander	2348
1	MS 0519	D. G. Thompson	2348
1	MS 0519	M. Thompson	2348
1	MS 0529	B. L. Remund	2340
1	MS 0529	B. L. Burns	2340
1	MS 0529	K. W. Sorensen	2345
1	MS 0529	B. C. Brock	2345
1	MS 0529	D. F. Dubbert	2345
1	MS 0529	S. S. Kawka	2345
1	MS 0529	G. R. Sloan	2345
1	MS 1207	C. V. Jakowatz, Jr.	5912
1	MS 1207	P. H. Eichel	5912
1	MS 1207	N. A. Doren	5912
1	MS 1207	I. A. Erteza	5912
1	MS 1207	T. S. Prevender	5912
1	MS 1207	P. A. Thompson	5912
1	MS 1207	D. E. Wahl	5912
1	MS 0507	B. C. Walker	2600
1	MS 0328	J. A. Wilder Jr.	2612
1	MS 0328	F. M. Dickey	2612
1	MS 1110	D. E. Womble	9214
1	MS 1110	L. A. Romero	9214
1	MS 1110	J. M. Delaurentis	9214
1	MS 9018	Central Technical Files	8945-1
2	MS 0899	Technical Library	9616
1	MS 0612	Review & Approval Desk for DOE/OSTI	9612
1		Randy Bell	DOE NNSA/NA-22